CORROSION
The Journal of Science and Engineering

Effect of test methods on corrosion phenomena of steel in highly resistive concrete systems and data interpretations

Journal:	*CORROSION*
Manuscript ID	CJ-2010-OA-3705.R2
Manuscript Type:	Original Article
Date Submitted by the Author:	n/a
Complete List of Authors:	Rengaraju, Sripriya; Indian Institute of Technology Madras, Civil Engineering Pillai, Radhakrishna; Indian Institute of Technology Madras, Department of Civil Engineering Gettu, Ravindra; Indian Institute of Technology Madras, Civil Engineering Neelakantan, Lakshman; Indian Institute of Technology Madras,
Key Words:	carbon steel, cracking, corrosion resistance, impressed current, Linear polarization resistance, corrosion monitoring, concrete

Effect of test methods on corrosion phenomena of steel in highly resistive concrete systems and data interpretations

Sripriya Rengaraju, Radhakrishna G. Pillai, ‡,* Ravindra Gettu,* and Lakshman Neelakantan ‡,**

‡Corresponding author. E-mail: pillai@civil.iitm.ac.in

*Department of Civil Engineering, Indian Institute of Technology Madras, Chennai, Tamil Nadu, India 600036.

**Corrosion Engineering & Materials Electrochemistry Laboratory, Department of Metallurgical and Materials Engineering, Indian Institute of Technology Madras, Chennai, Tamil Nadu, India, 600 036.

ABSTRACT

Fly ash and limestone calcined clay cement (LC3) are being used in concrete to enhance chloride resistance. In this study, 60 specimens (with steel in three separate binder systems, namely 100% OPC, 70% OPC + 30% fly ash, and LC3 with surface resistivity of ≈10, ≈25, and ≈200 kΩ.cm, respectively) were subjected to impressed corrosion and the results were compared with 15 lollipop steel-mortar specimens subjected to natural corrosion under wet-dry chloride environment. It was found that the traditional way of impressed corrosion tests can induce microstructural changes in highly resistive concrete cover and at steel-concrete interface; hence, are not suitable for evaluating corrosion resistance (such as corrosion rate and corrosion-induced cracking) in highly resistive concrete systems. Further, the Raman spectra from the corroded steel surfaces indicated that the impressed corrosion and natural corrosion tests led to different forms of corrosion (i.e., uniform and pitting, respectively) and different compositions of corrosion products (i.e., α-Fe_2O_3 and β–FeOOH phases). This led to different expansive stresses making the lab-to-field correlations inappropriate in case of highly resistive concrete systems. This paper recommends natural corrosion tests exposed to wet-dry conditions and not the impressed corrosion tests for assessing corrosion phenomena of steel in highly resistive concrete systems.

KEY WORDS: *Accelerated corrosion, composition of corrosion products, form of corrosion, impressed corrosion, limestone calcined clay (LC3) cement, Raman spectra, wet-dry.*

NOTATIONS AND ABBREVIATIONS

ρ	Resistivity of concrete
cov	Coefficient of variation
IC	Impressed corrosion
I_{corr}	Measured corrosion current (mA)
i_{corr}	Corrosion current density (μA/cm^2)
LC3	Limestone calcined clay cement
MIP	Mercury intrusion porosimetry
NC	Natural corrosion
OPC	Ordinary portland cement
PFA	70% OPC + 30% Class F Fly ash
R_p	Polarization resistance
S-B	Steel-cementitious binder
SCMs	Supplementary cementitious materials
SPS	Simulated pore solution
T_{crack}	Time-to-crack
TMT	Thermo-mechanically treated; also known as Quenched and self-tempered (QST)
w/b	Water to binder ratio

1 INTRODUCTION

The corrosion-free service life of reinforced concrete structures exposed to chlorides is dependent on the rate of chloride ingress through the cover concrete, and the physical and chemical characteristics of steel-cementitious binder (S-B) interface such as the presence of voids of different sizes and shapes, steel ribs, aggregates, cement chemistry (in particular, the lime rich layer in contact with the steel surface). The use of concrete with a compact and highly resistive microstructure can reduce the chloride ingress rate and hence, delay the corrosion initiation. Such high resistivity and pore refinement could result from the partial replacement of ordinary portland cement (OPC) with supplementary cementitious materials (SCMs) - leading to an increase in the chloride resistance and service life (Pillai et al., 2019). Figure 1 shows the range of electrical resistivity (collected from this study and literature) exhibited by OPC, fly ash + OPC, slag + OPC, fly ash + slag + OPC, silica fume + OPC, and LC3 systems (i.e., blend of clinker ≈ 50 %, limestone, and calcined clay) measured using a concrete cylinder without steel reinforcement (Dotto et al., 2004; Dhanya, 2015; Malakooti, 2017; Dhandapani et al., 2018). Table 1 shows the average and coefficient of variation of the resistivity of OPC, PFA and LC3 concretes (both M35 and M50 combined) used in this study and reported in Dhandapani et al. (2018). The higher the resistivity of concrete and the S-B interface, the lower will be the ionic flow between anodic and cathodic regions on the embedded steel, leading to lower corrosion rate and longer service life (Alonso et al., 1988; Hornbostel et al., 2013).

Many researchers adopt electrical methods (such as the application of potential difference) to accelerate the chloride ingress rate through concrete for indirectly assessing the corrosion characteristics of various S-B systems. This paper discusses the effect of the application of potential difference on the corrosion phenomena during the testing and hence, on the test results. In particular, the experimental results on the deviations (i.e., from natural corrosion) in the form, chemical composition, expansive nature of corrosion products and other effects that occur in the systems with high resistivity due to the application of potential difference are presented.

1.1 Effect of accelerated techniques on corrosion products

To obtain corrosion results in the short term, various laboratory techniques are used to accelerate the ingress of chlorides to the S-B interface and the corrosion process itself. Two of the techniques adopted for accelerating corrosion are immersion or cyclic wet--dry exposure using chloride solution and electrical methods. The possible effects of these techniques on the form and nature of corrosion products are discussed next.

1.1.1 Immersion and *cyclic wet-dry exposure to chlorides*

During immersion, the Cl^- ions move towards the S-B interface by diffusion, whereas in cyclic wet-dry exposure, the Cl^- ions move by capillary suction and diffusion. The chlorides occupy the O^{2-} vacancies in the passive film, and lead to the faster dissolution of iron and pit growth at those locations. The locations of the rebar with the pit acts as the anode, and the adjacent portions remain intact and act as the cathode, leading to localized corrosion (Montemor et al., 2003). This mimics natural field conditions and hence, the form of corrosion and corrosion products are similar to that in field structures (Angst et al., 2009). However, in the case of highly resistive concrete, the cyclic wet-dry exposure requires a long time for the ingress of sufficient chlorides to initiate corrosion; for example, in ASTM G109 tests using cyclic wet-dry exposure, corrosion initiation could take several years. Also, the macrocell (distinct anode and cathode) measurements taken across the top and bottom rebars in ASTM G109 specimens may not be indicative of ongoing microcell (anode and cathode change continuously and non-distinct) and macrocell corrosion between two points on the top bar itself (Hansson et al., 2006). Such macrocell corrosion with cathode and anode forming on the same rebar is the governing corrosion mechanism as the resistivity of concrete increases (Rengaraju, 2019). Because of these reasons and to accelerate chloride ingress, researchers have assessed the corrosion performance of steel by embedding it in mortar instead of concrete, which appears to be a good strategy to study the interface properties such as the chloride threshold in short period of time (Hussain and Ishita, 2011). Even for systems with pozzolans, it is possible to reduce

the testing period to a few months if mortar is used instead of concrete (Fajardo et al., 2009). Using mortar with reduced cover depth is another option to reduce the testing period for highly resistive cementitious systems, which is addressed in this paper.

1.1.2 Electrical methods

It has been reported that the use of electrical methods (i.e., application of potential gradient/current) to induce corrosion of steel in concrete systems with low resistivity would not affect the corrosion process significantly. For example, Care and Raharinaivo (2007) reported that an impressed current of 100 μA/cm^2 did not induce any changes in the nature of corrosion products formed on the steel when embedded in OPC mortar with low resistivity, compared to naturally occurring corrosion. However, in the case of highly resistive concrete systems, a high amount of applied current might be required to generate sufficient corrosion current at the S-B interface, which could lead to a significant deviation from corrosion under natural conditions. Hence, applying a constant external potential gradient is better than applying a constant external current in representing the driving forces in natural corrosion in S-B systems, which is in accordance with the procedures of several researchers (Sharkawi and Seyam, 2018; Narasimhulu et al., 2014; Abosrra et al., 2011; Sangoju et al., 2011; Austin et al., 2004). However, in the studies with constant potential gradient, the rebars are electrically connected to the anode terminal – forcing the entire rebar to be an anode, in which case, uniform corrosion occurs, as opposed to pitting corrosion that is predominant in natural chloride-induced corrosion (Yuan et al., 2007; Poursaee and Hansson, 2009). Furthermore, in the case of highly resistive concrete, the prolonged application of potential gradient is required, which could lead to changes in the microstructure – such as the forced-movement of Cl^- ions and hydroxyl ions towards the steel and that of Ca^{2+} and other cations away from the steel surface (Marcotte et al., 1999; Care and Raharinaivo, 2007). Such forced movements can result in increased porosity and interconnectivity of pores and the oozing of corrosion products, which in turn can reduce the expansive stresses and corrosion-induced cracking – although significant corrosion would have occurred (Marcotte et al., 1999). Though electrical methods have limitations, they are still widely used to assess the corrosion rate of various steel-concrete systems. Hence, there is a need to understand the possible changes in the corrosion phenomenon and the corrosion products formed due to this accelerated corrosion method in comparison with what happens in the natural, wet-dry induced corrosion in the field structures.

1.2 Other factors affecting corrosion products

The formation of different phases of iron and its hydroxides and oxides (such as α-, β-, γ-, and δ-FeOOH-, and γFe_2O_3) depends on the environmental conditions such as pH, temperature, and the availability of oxygen and moisture at the S-B interface (Misawa et al., 1974), which is summarized in Table 2. Figure 2 shows the relative magnitude of the expansion of the typical phases of iron oxides in chloride-rich environment (Hansson et al., 2012). The expansive stresses generated by the corrosion products, the porosity and pore structure of the S-B interface and surrounding concrete influence the flow of corrosion products, corrosion-induced cracking, and the time-to-crack, T_{crack} (Care et al., 2008). Nevertheless, the effect of the refined pore structure and higher resistivity in SCM-based concrete on the type of corrosion products, and their expansive nature are not well understood.

As mentioned earlier, the corrosion phenomena are dependent on the resistivity of the cementitious systems and the test method adopted. There is a need to categorize the material systems based on resistivity and suitable test methods, especially with the introduction of highly resistive concretes. This paper aims to study the corrosion phenomena on the steel embedded in cementitious systems with low to very high resistivity (such as OPC, PFA, and LC3 binders) when potential gradient and cyclic wet-dry exposure are used to drive the chlorides.

2 RESEARCH SIGNIFICANCE

Now-a-days, different types of concretes with highly resistive binders are being used to enhance the durability and reduce carbon footprint of reinforced concrete structures. However, researchers are continuing to use electrical methods for accelerating chloride ingress and study corrosion in such highly resistive concrete systems. This paper reports that the electrically impressed corrosion tests that are traditionally used for assessing corrosion of steel in low resistive concretes are not suitable for assessing corrosion of steel in highly resistive concretes. Such tests in highly resistive concretes need prolonged application of voltage, which can alter the microstructure of the concrete cover during the test and also lead to corrosion phenomena and corrosion products that are different from that observed in field structures. This paper provides cautions and guidelines for performing corrosion tests on steel in highly resistive concretes and obtaining results in short term –a few months. The findings in this paper can change the way corrosion tests are done on steel embedded in highly resistive cementitious systems.

3 OVERVIEW OF THE METHODOLOGY

Comprehensive experiments assessing the corrosion performance of steel embedded in three binder systems were conducted; the binders were OPC, PFA, and LC3, with the PFA system consisting of 70% OPC and 30% Class F fly ash, and the LC3 consisting of 50% OPC clinker, 31% calcined clay, 15% limestone and 4% gypsum. Quenched and self-tempered (QST) steel (known as thermo-mechanically treated (TMT) steel in the Indian sub-continent) was used for the study. Table 3 and Table 4 gives the chemical composition of the QST steel and the oxide composition of the binders used, respectively. The tests were conducted in two phases. Phase I involved impressed corrosion (IC) tests on concrete cylinders with embedded steel rebars in order to study the response with binders having OPC, PFA, and LC3. Major drawbacks of impressed corrosion tests were observed, especially on tests with highly resistive binders. Then, in order to understand the phenomena in detail, Phase II experiments were conducted by subjecting small mortar cylinders with embedded steel rebars to cyclic wet-dry exposure to chlorides. Then, the corrosion products from both IC and NC test specimens were analysed using the Raman Spectroscopy, and the effect of voltage application and resistivity of S-B binder types on the form and nature of corrosion products and resulting expansive stresses were analysed. Based on the key observations in the IC and NC tests and their comparisons, discussions are presented for evaluating corrosion phenomena and its consequences in reinforced concrete systems, especially with highly resistive concretes.

4 PHASE I – IMPRESSED CORROSION TESTING

4.1 Experimental program

The QST steel rebars were cleaned using an ultrasonic cleaner with an ethanol bath. Then, one end of the rebar was fastened to a stainless steel threaded rod of 4 mm diameter. The stainless steel all-thread was used to connect the QST steel to the lead wire of the DC power supply system. The embedded portion of the stainless steel was protected from crevice corrosion by using a heat shrink tube. The other end (in air) was connected to the lead wire. Two types of concrete (i.e., M35 and M50, denoting the characteristic cube compressive strength of 35 and 50 MPa, respectively) with the mixture proportions designed as per IS 456-2000 given in Table 5 were used to cast the specimens. All the concretes exhibited slump in the range of 100 ± 20 mm. Table 5 also gives the compressive and splitting tensile strength for each concrete. Cubes of 100 mm were used to determine the compressive strength; 150 mm diameter × 300 mm long cylinders were used for splitting tensile strength. Figure 3(a) and (b) show the schematic diagram and photograph of the IC test specimen and setup; each specimen was made of a concrete cylinder (200 mm long × 100 mm diameter) with a 16 mm diameter steel rebar (100 mm long) embedded at the centre; the end cover for the steel was 50 mm in order to provide axisymmetric

conditions with first cracking occurring radially due to the lower cover at the side (i.e., 42 mm). The specimens were cured for 28 days in a mist room at 25°C.

After the curing, each specimen was submerged in Simulated Pore Solution (SPS) with 3.5% NaCl; each litre of SPS contained 10.4 g of NaOH, 23.2 g of KOH, 0.3 g of $Ca(OH)_2$, and 966 g of distilled water (Pillai, 2009). SPS was chosen as the exposure solution to avoid leaching out of compounds such as $Ca(OH)_2$. The SPS is alkaline (pH = 12.6) with pH similar to that of cementitious system under testing. The stainless steel rod protruding out of the concrete was connected to the positive terminal, and the nickel chromium mesh placed in the electrolyte (counter electrode) was connected to the negative terminal of the DC power supply system set at 15 Volts. FM5 - 522 (2000) suggests to apply 6 V DC for accelerated corrosion testing. However, use of 6V would extend the test duration significantly, in particular for the case of LC3 with very high resistivity. Hence, to shorten the test duration, it was decided to maintain a high initial applied voltage of 15 V. ~~In order to avoid the heat generation in concrete and subsequent changes in microstructure, the potential gradient was applied for only 10 hours per day. Also, the duration of potential application i.e. 10 hours per day, facilitated the measurement of corrosion current readings every 4 hours with sufficient rest time in between, which avoided overheating of instruments as well.~~ In general, impressed current tests might experience some loss in voltage due to the ohmic resistance of the cover concrete (Hong et al., 2020). This voltage (15 V) was decided based on the traditional use in other studies and the assumptions in literature that most of the impressed current do participate in the corrosion reactions and negligible impressed current participate in the other reactions (Care and Raharinaivo (2007), Abosrra et al., 2011; Austin et al., 2004). In the present study, the voltage was applied at a rate of 10 hours per day in order to avoid overheating and temperature-induced changes in the microstructure of concrete. Then, using an Ammeter, as shown in Figure 3 (a), the corrosion current was measured at every four hours of voltage application and is considered as I_{corr}. As shown in Table 6, a total of 60 specimens (10 OPC, 20 PFA, and 30 LC3 specimens) were tested. In Group T1, all the three types of binders (OPC, PFA, and LC3) were included and the application of potential gradient was terminated in PFA and LC3 companion specimens when the OPC specimens cracked. In Group T2, only the PFA and LC3 specimens were included, and when the PFA specimens exhibited cracking, the testing of companion LC3 specimen was also terminated. In Group T3, only LC3 specimens were tested until 500 hours of potential application.

At the end of the IC tests, the cylindrical specimens were split into halves by applying a compressive load on the curved surface, the steel rebars were extracted and examined visually to identify the form and extent of corrosion damage. The extracted steel piece was immediately placed under Raman microscope and the spectra from the corrosion products on the steel surface was collected. Because this was done immediately, the chances of further oxidation of the corrosion products is limited. A monochromatic light with a 488 nm wavelength and 600 gratings (with a Horiba Jobin Yvon HR 800 UV instrument) was used, and the spectra obtained were compared with literature for specific peaks to identify the oxide phases present. Then, the steel specimens were cleaned using ASTM G1 solution (mixture of 500 ml HCl, 3.5 g of hexamethylene tetramine, and 500 ml distilled water) and the form and extent of corrosion was visually observed. In addition, the porosity of the M35 concrete was also determined on small pieces of mortar (1 g) collected from three locations along the 100 mm long S-B interface, using mercury intrusion porosimetry (MIP) [with a Thermo Scientific, Pascal 140 – 440 Porosimeter].

4.2 Effect of resistivity of concrete on corrosion current

Figure 4 shows the corrosion current (I_{corr}) measured on the specimens of M35 and M50 concretes in the T1, T2, and T3 groups. In the T1 group with M35 concrete, the first OPC specimen cracked at about 160 hours. When OPC specimen cracked, testing of companion specimens (both PFA and LC3) was stopped. In this way, when all the OPC specimens cracked, further voltage application on all the other specimens was terminated. As shown in Figure 4 (a), the OPC, PFA, and LC3 specimens exhibited three distinct ranges of I_{corr} – depending on the resistivity, ρ, of concrete. For

the OPC concrete (ρ ≈ 10 kΩ.cm), the I_{corr} values ranged from 40 to 80 mA, for the PFA concrete (ρ ≈ 25 kΩ.cm) it ranged from 10 to 30 mA, and for LC3 concrete, with significantly high resistivity (ρ ≈ 250 kΩ.cm; Dhandapani and Santhanam, 2017), it was significantly low (i.e., < 3 mA). Figure 4 (b) shows the I_{corr} of PFA and LC3 specimens in Group T2 (with M35 concrete), where PFA specimens cracked at about 250 hours, at which the testing of companion LC3 specimens was also terminated. Figure 4 (c) shows the I_{corr} data for Group T3 consisting of only LC3 specimens with M35 concrete, where none of them cracked even after 500 hours of potential application, indicating very good resistance against corrosion-induced cracking. This kind of 3-step experimental program was designed to bring out the corrosion resistance of SCM-based concretes due to their higher resistivity, which prevents the ingress of chloride ions. Also, the highly resistive concrete reduces the impressed potential (due to ohmic drop across the highly resistive cover concrete) to reach the steel surface to cause impressed corrosion.

As evident from Figure 4 (d), (e) and (f), all M50 concrete with OPC and PFA exhibited lower I_{corr} and delayed cracking (about twice the time for M35 concrete). In the T1 group with OPC, PFA, and LC3 specimens, the OPC specimens cracked at about 380 hours; in the T2 group with PFA and LC3 specimens, the PFA specimens cracked at about 430 hours; and in the T3 group with only the LC3 specimens, no cracking was visible even until 500 hours. In general, the T_{crack} is in the order of LC3 >> PFA > OPC for both the M35 and M50 concretes studied, with the OPC, PFA and LC3 specimens exhibiting severe, hairline and no visible cracks, respectively (see Figure 5). Since the cover depth, compressive strength grade and splitting tensile strength of all the concretes were similar, it can be concluded that the difference in I_{corr}, T_{crack}, and crack conditions are governed by the resistivity of concrete, ρ. It is interesting to note that AASHTO (AASHTO T 358 (2017)) has classified the concretes based on their surface resistivity (See Figure 1). According to this classification, any cementitious system having ρ > 37 kΩ.cm, irrespective of the binder formulation and w/b, has higher resistance against chloride ingress. Consequently, LC3 systems, which exhibit very high resistivity (> 250 kΩ.cm), have low I_{corr} and delayed T_{crack}.

4.3 Effect of binder types on forms of corrosion

Figure 6 (a) shows photographs of a rebar piece extracted from an OPC specimen after 160 hours of voltage application, and of the same piece after cleaning with ASTM G1 solution and with high contrast to highlight the corrosion pits and striations. Figure 6 (b) and (c) show similar photographs of steel from the PFA and LC3 specimens after 250 and 500 hours of voltage applications, respectively. The OPC and PFA specimens exhibited pits and a majority of the surfaces had uniform corrosion; the corrosion products were highly oxidised (black or dark brown). Visible striations were observed on the surface of steel embedded in OPC - indicating higher corrosion current than PFA and LC3 specimens. Pits were observed on the steel embedded in OPC and PFA at locations due to the presence of voids/initiation of microcracks. In the LC3 specimens, only a thin layer of orange-brown corrosion products was observed, which did not lead to any visible cracking.

4.4 Effect of impressed voltage on composition of corrosion products

Figure 7 shows the Raman spectra obtained from the corrosion products of steel in OPC, PFA, and LC3 concretes (after the IC test). As recommended by Oh et al. (1998), a tolerance of ±10 cm^{-1} in the Raman shift is considered while analysing the spectra from the non-homogeneous and porous S-B interface. It is seen that corrosion products such as α-FeOOH, γ-FeOOH are observed in the OPC systems with high pH, and not in PFA and LC3 systems with low pH environment. Figure 7 (b) indicates the presence of Fe_3O_4 (peaks at 532 and 667 cm^{-1}) and δ-FeOOH (peaks at 297, 392, 666 cm^{-1}) in the PFA systems, with the presence of δ-FeOOH indicates the presence of negligible chloride concentration at the steel surface. Consequently, the early cracking in the OPC and PFA systems can be attributed to the expansive nature of the corrosion products and the high corrosion rates due to low resistivity. Figure 7 (c) indicates the presence of α-Fe_2O_3 (hematite; two peaks at 226 and 292 cm^{-1}) in the LC3 systems. Hematite is a stable phase with less surface area, high compactness (due to its relatively dry state), and about twice the volume of steel. The expansive

pressure induced by hematite is, therefore, less than that induced by the other stable oxides and hydroxides of iron (Care et al., 2008). Further, in LC3, the hematite is accompanied by magnetite (peaks at 532 and 667 cm^{-1}), the combination of which is similar to the passive layer. The presence of hematite could either indicate the presence of an intact passive layer or the absence of moisture in phase transformations (e.g., from goethite to hematite), both of which limit the volumetric expansion in LC3, leading to a delay in corrosion-induced cracking.

4.5 Effect of binder type on the pore structure of S-B interface

Depending on the pore structure of the S-B interface region, the corrosion products can either accumulate in the interface region resulting in the build-up of radial pressure, which can cause the cover to crack, or move away from the S-B interface through interconnected pores. Figure 8(a) and (b) show the specific pore volume and the differential intrusion volume at the S-B interface in the M35 systems with the three binders, which gives information on the threshold diameter, and critical pore size. The threshold diameter is the minimum continuous pore size of the sample, which can be obtained from the cumulative volume intrusion curve by intersecting tangents at the smallest diameter and the largest diameter. The critical pore size is obtained from the peak in the differential intrusion volume curve (Figure 8(b)), which indicates the size corresponding to the maximum volume intrusion

For LC3, the threshold diameter and critical pore size are about 0.1 and 0025 μm, respectively. Also, as indicated by the two peaks of the solid curve in Figure 8 (b), the major pore diameters for LC3 are about 0.01 and 0.025 μm. Such small pore diameters indicate the presence of either interconnected gel pores within calcium silicate hydrate (C-S-H) and calcium alumino silicate hydrate(C-A-S-H), or discrete well-refined capillary pores. In the former case, the gel pores in C-S-H and C-A-S-H adsorb the ions in the pore solution as explained earlier and are not free to move easily; whereas, in the latter case, the tortuosity can lead to a longer path for ionic movement (San Nicolas et al., 2014). Both these conditions are favourable for hindering ionic movement, which could explain the lower corrosion rate in LC3 systems due to the formation of less expansive hematite. Also, some of the corrosion products formed could occupy the pores at the S-B interface without creating pressure as LC3 is seen to have higher pore volume than the other binder systems. Hence, it can be concluded that the pore structure and less expansive corrosion products (such as hematite) formed in LC3 systems delay the corrosion-induced cracking.

The threshold diameter in PFA concrete was about 0.4 μm and the critical pore size was about 0.07 μm. Figure 8 (b) shows that the PFA concrete also had multiple peaks indicating major pore diameters of about 0.01 and 0.07 μm – gel pores within C-S-H or capillary pores. OPC systems exhibited a threshold diameter of about 0.8 μm and critical pore diameter of size 0.04 μm. However, the electrical resistivity of OPC was much less than that of PFA systems, leading to faster ingress of chlorides and moisture in the former than the latter. Hence, the corrosion rate in OPC was higher than that in PFA. Also, due to the buffering of calcium hydroxide from the regions near the interface, the restructuring and coarsening of pores could have taken place at the S-B interface in OPC systems, before severe corrosion and cracking (Alonso et al., 1998). All these phenomena leads to corrosion products with expansive nature in OPC systems. However, due to less calcium hydroxide, the buffering action is less in PFA and leads to less coarsening of pores. Also, the degree of such corrosion reactions and the amount of expansive products are relatively lower in PFA and LC3 systems due to the higher chloride resistance. Moreover, in LC3 systems, the early hydration refines the pore structure to a greater extent resulting in lower corrosion current than that in PFA.

4.6 Effect of impressed voltage on the bulk concrete cover

As mentioned before, the OPC specimens exhibited corrosion-induced cracking at an earlier time than PFA specimens. However, LC3 concrete specimens did not crack even after about 500 hours of voltage application. Hence, for LC3 specimens, to further accelerate the testing, the voltage application regime was changed from Regime 1 (with 10 hours of voltage application followed by 14 hours of rest period in a day) to Regime

2 (with 4 hours of voltage application followed by 0.5 hours of rest period). However, the prolonged application of impressed voltage eventually led to microstructural changes in the bulk of the concrete cover. This was demonstrated by the oozing out of green spongy material from the surface of the concrete. This spongy material left the concrete surface and started floating on the exposure solution (see Figure 9), which turned to white upon atmospheric exposure for a few minutes and settled down.

This oozing out of spongy material from the bulk of concrete could have created micropores in the concrete cover and at the steel-concrete interface. This in turn led to the movement of corrosion products away from steel surface, exposing new surfaces of steel underneath and further impressed corrosion. However, the measured current values of LC3 specimens did not show any increase even after the oozing out of corrosion products were observed. ~~Also, the steel in LC3 specimens experienced significant mass loss that is comparable to steel in OPC and PFA specimens~~. As a result of this outcome, a new set of specimens were cast and subjected to 60 V (cyclic voltage application of 10 hours followed by 14 hours of rest period daily) till the appearance of crack on the concrete surface. The reasoning behind increasing the voltage from 15 to 60 V was that the steel embedded inside the highly resistive concrete could not have experienced sufficient driving force to induce corrosion – due to the high resistance offered by the thick concrete cover. However, the application of 60 V led to the heating of the specimens (with steel and concrete) and release of fumes from the SPS immersion solution. This also led to the corrosion of electrical lead wires and the testing had to be stopped.

It should be noted that the voltages in the range of 60 V is applied for just 6 hours in the conventional chloride penetration resistance tests (such as ASTM C1202) that use concrete plain concrete cylinder specimens. However, in case of steel in highly resistive concretes (where surface resistivity > 37 kΩ.cm), prolonged application of voltage is required, which can lead to voltage-induced changes at the steel-concrete interface; and must be avoided in laboratory tests. Hence, electrical methods are not recommended for testing corrosion initiation and corrosion-induced cracking in concrete with highly resistive systems.

In summary, impressed current led to different rates of corrosion in OPC, PFA, and LC3 systems. Moreover, although the time-to-cracking was different in these specimens, ~~their corresponding mass loss was similar,~~ which was not reflected by the current measurements and not correlated to the crack pattern. This indicates (i) the possible changes in the microstructure of highly resistive cover concrete due to prolonged current application and (ii) the differences in the expansive nature of corrosion products, which is dependent on its form and composition – leading to different tendencies for corrosion-induced cracking. The highly resistive LC3 systems exhibited negligible cracking as opposed to significant cracking in low to moderately resistive OPC and PFA systems. These show the inadequacy of impressed corrosion test methods for assessing steel in highly resistive concrete systems such as LC3. This led to the Phase II experiments with natural corrosion tests on steel in highly resistive cement mortar with less cover than that in Phase I and subjected to cyclic wet-dry exposure to chlorides. The results from Phase I and II will be compared later.

5 PHASE II: NATURAL CORROSION TESTS AND RESULTS

5.1 Experimental program

As shown in Figure 10, lollipop-type test specimens were prepared for the natural corrosion (NC) tests. Each specimen had an 8 mm diameter and 100 mm long steel rebar embedded in a cylindrical mortar (with 10 mm side cover). The rebars were cleaned using an ultrasonic cleaner with ethanol as immersion solution. The OPC, PFA, and LC3 mortars (5 specimens each) were made with water:binder:sand ratio of 0.5:1:2.75. Grade 2 (0.5 – 1 mm size) and Grade 3 sand (90 – 500 μ size) conforming to IS 650 –1991 (R2008) were used for mortar study. After 28 days of curing in a mist room, the specimens were coated with two thin layers of low viscosity epoxy (Sikadur-52 UF) leaving 50 mm at the centre to restrict the area of

exposure as shown in Figure 10 (a). Once the epoxy coating was tack-free, the specimens were subjected to cyclic wet-dry regime following 2 days wet in 3.5 % NaCl +SPS solution and 5 days dry at 25 °C and 65 ± 5 % RH.

Then, a three-electrode corrosion cell setup, as shown in Figure 10 (b) and (c), with a working electrode (WE), a counter electrode (CE), and a reference electrode (RE) was prepared. The uncoated region (50 mm) of the steel piece was considered as the WE. A 90 mm diameter pipe made of Nichrome wire mesh was used as the CE and the test specimen was placed inside this CE. For clarity, this CE is not shown in the photograph in Figure 10 (c). The saturated calomel electrode (SCE) was used as the RE and placed close to the surface of mortar (gap being double that of the tip diameter; as per Rengaraju et al., 2019). All the electrodes were placed in a glass beaker with 3.5% NaCl +SPS solution. This formed the corrosion cell, which was then connected to a potentiostat and computer for recording the repeated electrochemical measurements (i.e., potentiodynamic linear polarization resistance (LPR)) during the cyclic wet-dry exposure. At the end of each wet period, LPR was measured using a scan range of ±10 mV Vs. OCP and a scan rate of 0.05 mV/s that have been chosen considering the wide range of the resistivity of the mortars used (Rengaraju et al., 2019).

Figure 11 shows a typical linear polarization curve. The steeper the curve when crossing the zero-current axis, the larger will be the instantaneous corrosion current density, i_{corr}. The i_{corr} at the end of every wet period was calculated using the data from LPR tests and Eq. (1).

$$i_{corr} = \frac{B}{R_p} = \frac{B}{\left(\Delta E / \Delta i\right)_{E \to E_{Corr}}} \quad \text{Eq. (1)}$$

where, B is the Stern Geary constant (26 mV –(Andrade and Gonzalez,1978; Kranc and Sagues, 1993; Poursaee, 2016)), R_p is the polarization resistance of steel ($\Omega.cm^2$), ΔE is the applied potential (Volts), Δi is the measured corrosion current density (A/cm^2), E is the potential and E_{corr} is the equilibrium potential/corrosion potential of the specimen. The slope of the polarization curve (see Figure 11) at E_{corr} is considered as R_p. Here, LPR without current interruption was used because of the limitation of the electrochemical system for the adopted corrosion cell. Further details are presented elsewhere (Rengaraju et al., 2019)

The initiation of active corrosion was detected using a statistical procedure that identifies when there is a significant increase in the i_{corr} as compared to a stable i_{corr} data. To define the stable data, the mean (μ_{st}) and standard deviation (σ_{st}) of five consecutive readings of $1/R_p$ were calculated, such that each individual reading falls within ($\mu_{st} \pm 1.5\sigma_{st}$) value. Once the stable data was identified, the specimens were continued with the monitoring and considered to be initiated when $1/R_p$ crosses the value ($\mu_{st} + 3\sigma_{st}$). More details of the test procedure can be found in Karuppanasamy and Pillai (2017) and Rengaraju (2019). Upon corrosion initiation, the specimens were split into two and examined visually. Later, the corrosion products were characterised by Raman Spectroscopy.

5.2 Effect of resistivity of mortar on corrosion current density

The pore structure of the hardened cement paste collected from the OPC, PFA, and LC3 concretes were obtained using Mercury Intrusion Porosimetry (MIP) and provided in Figure 8. This can be similar to the hardened cement paste of the mortar used in this study because the water-binder ratio is similar in mortar and concretes used. Hence, the effects on corresponding resistivity is also similar. Figure 12 shows the i_{corr} for steel in OPC, PFA and LC3 systems (at the end of each wet period). The OPC and PFA specimens exhibited similar current and the initiation of active natural corrosion earlier than the LC3 specimens. Throughout the testing period, the i_{corr} values in the LC3 specimens were lower than that in OPC and PFA systems, which can be attributed to the higher resistivity of the LC3 systems, especially at the S-B interface - due to early hydration and pore

refinement. ~~As discussed in Section 4.6,~~ In LC3 systems, the high resistivity of the mortar cover and the steel-mortar interface can mask the severity of the ongoing corrosion, as observed in the ~~electrochemical~~ measured $1/R_p$ readings. Hence, the absolute failure criteria applicable for low resistive systems like OPC such as E_{corr} < -350 mV vs. CSE (ASTM C876), i_{corr} > 0.1 μA/cm^2 (RILEM TC 154-EMC) etc. were not adopted in this study. Instead, the failure criteria based on a statistically significant increase in $1/R_p$ as compared to a stable $1/R_p$ data (as defined earlier) was adopted to eliminate the possible masking of corrosion activity and misleading interpretations of the electrochemical readings.

5.3 Effect of spatial variation of chlorides on the form of corrosion

The form of corrosion in steel can depend on its immediate environment and the physical and chemical nature. In the Impressed Corrosion tests in Phase I, the steel in OPC, PFA, and LC3 specimens exhibited uniform corrosion (see Figure 6). However, in the Natural Corrosion tests (in this phase), a pattern of localized chloride-induced corrosion was observed (see Figure 13). The steel rebars did not show any general/uniform corrosion products and were pristine, except for the pit locations. In case of mortar with fine aggregates, the chlorides can diffuse through the pore solution, interfacial transition zones between the fine aggregates and hardened cement phase, interconnected pores, etc., leading to an uneven distribution of chlorides at the steel surface at a particular time instant, which can also vary depending on the tortuosity, anion-cation ratio and pore distribution (Angst and Polder, 2014). Also, the LC3 systems exhibited refined pore structure with lesser capillary pores from the early age itself (Dhandapani and Santhanam, 2017). This increased the resistivity and is evident from the low measured corrosion current density in LC3 systems. In the early stages, the resistivity of OPC and PFA systems was in similar order of magnitude (about 100 to 200 Ω); whereas that of LC3 was one order of magnitude higher (about 1500 Ω). and hence, the electrochemical readings of the steel in OPC and PFA systems were similar. Also, the finer pore structure and the presence of fine aggregates lead to more tortuous path for the ionic/fluid ingress (chloride ingress). This spatial variation in the chloride ingress rate leads to variations in the instantaneous chloride concentrations at the steel surface, which in turn also results in the initiation of localized and pitting corrosion at specific locations (i.e., wherever the chloride concentration is above the chloride threshold) and subsequent propagation, if the microclimate favours.

5.4 Effect of chlorides at S-B interface on composition of corrosion products

The Raman spectra shown in Figure 14 indicate that in OPC specimens, both α-FeOOH and β-FeOOH were observed at the pit locations. The Raman spectra obtained from PFA and LC3 specimens also indicate the presence of β-FeOOH at the pits, indicating chloride-induced corrosion. Irrespective of the type and resistivity of the binder, when the chlorides accumulate at steel interface and reaches a critical threshold value, it leads to pitting corrosion and the presence of β-FeOOH confirms the cause of corrosion initiation as chlorides (as per the reasoning by Marcotte et al. (2007). The adoption of wet-dry exposure to chlorides led to the formation of corrosion product with similar composition as that found in the natural corrosion in field structures. It should be noted that during the cyclic wet-dry exposure, the acceleration of chloride ingress is happening via diffusion and leads to natural corrosion. However, in the impressed corrosion tests, the applied voltage is directly accelerating the corrosion leading to changes in the composition of corrosion products than that found in field structures. It is confirmed that, unlike the impressed corrosion tests, the natural corrosion tests using wet-dry exposure to chlorides can mimic the scenario on the field structures and hence, suitable for all kinds of cementitious systems, irrespective of their resistivity.

5.5 Summary – Phase II

The spatial variation of instantaneous chloride concentrations at the steel surface (due to the tortuosity of the ingress path in the bulk mortar cover) and in the physical nature of the S-B interface can lead to pitting corrosion even in highly resistive concrete systems like LC3. However, the measured corrosion current density (before and at the time of corrosion initiation) was low in LC3 system compared to OPC and PFA systems due

to the difference in the resistivity of the cover and S-B interface between OPC, PFA and LC3. This emphasizes that the resistivity of the mortar cover must be considered while interpreting the electrochemical data, especially from steel in highly resistive cementitious systems; unlike metal-aqueous systems.

6 DISCUSSION - EFFECT OF TEST PROCEDURES

Sections 4 and 5 presented the results from the impressed corrosion (IC) and natural corrosion (NC) tests, respectively, on steel in OPC, PFA, and LC3 systems. This section compares the major differences in the form and composition of corrosion products observed in IC and NC tests. Table 7 summarizes these results indicating that the corrosion phenomena due to wet-dry exposure to chlorides is different from that due to the application of voltage. Figure 15 shows a schematic on the comparison of the electrochemical driving forces and the resulting corrosion phenomena in IC and NC tests. The wetting and drying process in NC tests accelerates the ingress of chlorides; whereas, the voltage application in IC tests impresses corrosion directly. In the case of IC tests, the entire surface of the steel rebar experiences similar driving forces due to the potential difference (or voltage) applied; and hence, experiences uniform corrosion (see Figure 15(a)) until the concrete cover cracks. Also, the composition of corrosion products formed in this case is different from that observed in the field structures; and hence, the expansive pressure induced could also be different. Also, the steel can corrode without the presence of chlorides at the S-B interface and due to the acidification of the S-B interface as a response to the applied voltage. These does not represent the condition in the field structures.

In this case of NC tests, the chlorides ingress through a tortuous path in the mortar cover and reach the steel surface in various quantities - leading to simultaneous depassivation at various points, where the passive film is weak and chloride concentrations are above the threshold. This leads to the typical pitting corrosion (see Figure 15(b)) found in steel-concrete systems. The pitting corrosion products can then move along the S-B interface, as shown in Figure 15 (b). As more corrosion products are formed, they tend to exert similar expansive pressure (because of similar composition of corrosion products as in the field structures) onto the surrounding concrete - similar to what happens in the field structures. This phenomenon can be magnified in case of concrete due to the presence of coarse aggregates. The presence of coarse aggregates can induce significantly high resistivity and highly tortuous path for chloride ingress. Hence, the chloride concentration causing pitting corrosion can be spatially distributed. Nevertheless, the chloride threshold and the initiation parameters are a function of the interface properties, which are well captured in this study using steel embedded in mortar.

It is important that the test procedures adopted mimic the conditions in the field structures so that the obtained results can be applied to the field. The primary motivation behind conducting the IC tests is comparing the performance of different binders against corrosion resistance by comparing the time taken for the cracking of cover concrete. However, such comparison is possible even in the chloride migration test as it works on the same principle of voltage application. On the other hand, if the IC tests are performed to obtain the corrosion rate, there may be chances of misinterpretation of data, especially in the case of highly resistive concrete systems (surface resistivity > 37 kΩ.cm). Considering the fact that IC tests on steel in highly resistive concretes need prolonged application of voltage, which can change the microstructure of the concrete cover during the testing period, and lead to a different form of corrosion than what is observed in the field, the IC tests are not recommended to study corrosion phenomena of steel in highly resistive concrete systems like LC3 and its consequences such as cracking.

The corrosion products (α-FeOOH, γ-FeOOH, δ-FeOOH) formed in OPC and PFA concretes (see Table 7) after IC tests indicate the formation of oxides without the presence of chlorides. These oxides form due to the impressed voltage forcing the dissolution of steel (i.e., corrosion). Because of the formation of these oxides, there will be an expansive force, which exerts radial pressure causing the concrete cover to crack. This was visible

in the cases of OPC and PFA concretes (see Figure 5). However, in LC3 system with high resistivity, the steel surface might not have experienced the same level of applied current as in low resistivity concretes (although the voltage is same). Hence, the iron oxide formed on steel in highly resistive concrete is similar to that of passive film with hematite and magnetite. Since the passive film is intact, there is no radial pressure for the concrete cover and hence, the LC3 concretes did not crack even after the application of voltage (15 V) for 500 hours. It should be noted that the LC3 specimens had similar behaviour for both M35 and M50 concrete. However, in the case of natural corrosion tests, β-FeOOH is formed irrespective of the binder type (see Table 7). It should be noted that the presence of α-FeOOH along with β-FeOOH in the pit location indicates that there was a formation of additional corrosion products due to the ongoing reactions and does not necessarily indicate uniform corrosion. The pitting corrosion is predominant in the case of natural corrosion subjected to wet-dry exposure and is stochastic in nature. The corrosion initiation happens at the locations, where the passive film is weak and the chloride concentration is higher than the chloride threshold. This is not usually the case with uniform corrosion, which can occur predominantly in the presence of moisture and low pH. The presence of β-FeOOH indicates that the corrosion is caused due to the presence of chloride and is similar to what could happen in field structures – hence, recommended for studies on corrosion assessment of steel in highly resistive concretes.

To summarize, the nature of exposure condition and the source of driving forces has high impact on the form of corrosion and the composition of corrosion products. The IC test was inadequate to assess the corrosion performance in highly resistive systems as the corrosion phenomenon (uniform corrosion with less expansive corrosion products) is different than in natural corrosion (pitting corrosion with β-FeOOH). Hence, it can be concluded that the test procedures influence the corrosion mechanism and should be carefully chosen – to avoid deviation from the natural corrosion phenomena in field structures; and hence, to avoid erroneous conclusions on the consequences of corrosion.

7 CONCLUSIONS

Impressed corrosion (IC) and natural corrosion (NC) tests were conducted on steel in cementitious systems with various levels of resistivity. It was found that IC and NC tests lead to different forms of corrosion and compositions of corrosion products with different expansive properties. It is also found that such differences are more evident in the highly resistive cementitious systems with limestone calcined clay cement (LC3).

- The IC test induces uniform corrosion as the application of potential or voltage forces the entire length of steel to act as anode, and the corrosion can occur even without the presence of chlorides at the steel surface.
- The IC tests on steel in highly resistive concretes need prolonged application of voltage, which can alter the microstructure of the concrete cover during the testing period and lead to different forms of corrosion than what is observed in the field.
- When the surface resistivity of concrete is greater than 37 kΩ.cm, the IC tests are not suitable for evaluating corrosion phenomena of steel in concretes and corrosion-induced cracking.
- During the NC tests, the chlorides can ingress through the tortuous paths in the cover concrete and accumulates on the steel surface. Because of the spatial variations in the instantaneous chloride concentrations, the embedded steel experiences localized corrosion (pitting) at various locations, where the chloride concentration is above the threshold.

- The composition of the observed corrosion products after NC tests indicate similarity with the natural corrosion products found in field structures. Hence, NC tests on steel embedded in mortar cylinder and exposed to cyclic wet-dry conditions can be adopted for evaluating corrosion phenomena and corrosion initiation characteristics of steel in highly resistive concretes (surface resistivity > 37 kΩ.cm).

8 ACKNOWLEDGMENTS

This research is partially funded by the Limestone Calcined Clay (LC3) project – Phase I (Project Number: 7F-08527.02.01) sponsored by the Swiss-Agency for Development and Cooperation, Switzerland. The authors also acknowledge the financial support received from the Department of Science and Technology (Sanction No. EMR/2016/003196) and the Ministry of Human Resources Development, Government of India, through Indian Institute of Technology Madras (IITM), Chennai. Also, the authors express their gratitude to the staff and researchers in the Construction Materials Research Laboratory (CMRL), Department of Civil Engineering, IITM, Chennai, India.

9 REFERENCES

1. Abosrra, L., A.F. Ashour, and M. Youseffi, *Constr. Build. Mater.* 25 (2011): pp. 3915–3925,
2. Alonso, C., C. Andrade, and J.A. Gonzalez, *Cem. Concr. Res.* 18 (1988): pp. 687–698.
3. Alonso, C., C. Andrade, J. Rodriguez, and J.M. Diez, *Mater. Struct.* 31 (1998): pp. 435–441,
4. American Association of State Highway and Transportation Officials (AASHTO), Washington, D.C., USA, 2017, AASHTO T 358-17
5. Andrade, P.C., C. Alonso, R. Polder, R. Cigna, O. Vennesland, M. Salta, A. Raharinaivo, and B. Elsener, *Mater. Struct.* 37 (2005): pp. 623–643.
6. Andrade, C., and J. A. Gonzalez,.Mater. Corros., 29(8) (1978): pp. 515–519.
7. Angst, U., B. Elsener, C.K. Larsen, and Ø. Vennesland, *Cem. Concr. Res.* 39 (2009): pp. 1122–1138
8. Poursaee, A., Corrosion of Steel in Concrete Structures, Corrosion of Steel in Concrete Structures (Elsevier Ltd, 2016).
9. Kranc, S.C., and A.A. Sagüés, *J. Electrochem. Soc*. 144 (1997): pp. 2643–2652.
10. Angst, U.M., and R. Polder, *Cem. Concr. Res.* 56 (2014): pp. 40–51.
11. ASTM International, West Conshohocken, PA, USA, 2011, ASTM G1-11.
12. ASTM International, West Conshohocken, PA, USA, 2013, ASTM G109-07.
13. ASTM International, West Conshohocken, PA, USA, 2015, ASTM C876-15.
14. Austin, S.A., R. Lyons, and M. Ing, *Corrosion* 60 (2004): pp. 203–212.
15. Caré, S., and A. Raharinaivo, *Cem. Concr. Res.* 37 (2007): pp. 1598–1612.
16. Care, S., Q.T. Nguyen, V. L'Hostis, and Y. Berthaud, *Cem. Concr. Res.* 38 (2008): pp. 1079–1091.
17. Criado, M., S. Martínez-Ramirez, and J.M. Bastidas, *Constr. Build. Mater.* 96 (2015): pp. 383–390.
18. Dhandapani, Y., and M. Santhanam, *Cem. Concr. Compos.* 84 (2017): pp. 36–47.
19. Dhandapani, Y., T. Sakthivel, M. Santhanam, R.Gettu and R.G.Pillai, *Cem. Concr. Res.* 107 (2018): pp. 136–151.
20. Dhanya B. S., "Study of the influence of supplementary cementitious materials on selected durability parameters of concrete" (Ph.D. diss., Indian Institute of Technology Madras, 2019)
21. Dotto, J.M.R., A.G. De Abreu, D.C.C. Dal Molin, and I.L. Müller, *Cem. Concr. Compos.* 26 (2004): pp. 31–39.
22. Fajardo, G., P. Valdez, and J. Pacheco, *Constr. Build. Mater.* 23 (2009): pp. 768–774.
23. Florida Department of Transportation (FDOT), Gainesville, Florida, USA, FM5 - 522 (2000)
24. Hansson, C.M., A. Poursaee, and A. Laurent, *Cem. Concr. Res.* 36 (2006): pp. 2098–2102.
25. Hansson, C.M., A. Poursaee, and S.J. Jaffer, *The Masterbuilder* (2012).
26. Hong, S., F. Zheng, G. Shi, J. Li, X. Luo, F. Xing, L. Tang, B. Dong, *Cem. Concr. Compos.* 108 (2020): 103536
27. Hornbostel, K., C.K. Larsen, and M.R. Geiker, *Cem. Concr. Compos.* 39 (2013): pp. 60–72.
28. Hussain, R.R., and T. Ishida, *KSCE J. Civ. Eng.* 15 (2011): pp. 153–160.
29. Karuppanasamy, J., and R.G. Pillai, *Mater. Struct.* 50 (2017): pp. 1–17.
30. Malakooti, A. "Investigation of concrete electrical resistivity as a performance based test" (M.S. Thesis., Utah State University, Utah, USA, 2017).
31. Marcotte, T.D., and C.M. Hansson, *Mater. Struct.* 40 (2007): pp. 325–340.
32. Marcotte, T.D., C.M. Hansson, and B.B. Hope, *Cem. Concr. Res.* 29 (1999): pp. 1561–1568.

33. Misawa, T., K. Hashimoto, and S. Shimodaira, *Corros. Sci.* 14 (1974): pp. 131–149.
34. Montemor, M.F., a. M.P. Simões, and M.G.S. Ferreira, *Cem. Concr. Compos.* 25 (2003): pp. 491–502.
35. Narasimhulu, K., R. Gettu, and K.G. Babu, *J. Mater. Civ. Eng.* 26 (2014): pp. 24–33.
36. Oh, S.J., D.C. Cook, and H.E. Townsend, *Hyperfine Interactions* 112(1998): pp 59–66
37. Pillai, R.G., "Electrochemical characterization and time-variant structural reliability assessment of post-tensioned, segmental concrete bridges" (Ph.D. diss., Texas A&M University, Texas, USA, 2009)
38. Pillai, R.G., R. Gettu, M. Santhanam, S. Rengaraju, Y. Dhandapani, S. Rathnarajan, and A.S. Basavaraj, *Cem. Concr. Res.* 118 (2019): pp. 111–119.
39. Poursaee, A., and C.M. Hansson, *Cem. Concr. Res.* 39 (2009): pp. 391–400.
40. Rengaraju, S., A.Godara, P. Alapati, and R.G. Pillai, *Mag. Concr. Res.* (2018): pp. 1–32.
41. Rengaraju, S. "Electrochemical Response and Chloride Threshold of Steel in Highly Resistive Concrete Systems" (Ph.D. diss., Indian Institute of Technology Madras, 2019).
42. Rengaraju, S., L. Neelakantan, and R.G. Pillai, *Electrochim. Acta* 308 (2019): pp. 131–141.
43. Sagoe-Cretsil, K.K., and F.P. Glasser, *Corrosion* 49 (1993): pp. 457–463.
44. San Nicolas, R., M. Cyr, and G. Escadeillas, *Constr. Build. Mater.* 55 (2014): pp. 313–322.
45. Sangoju, B., R. Gettu, B.H. Bharatkumar, and M. Neelamegam, *J. Mater. Civ. Eng.* 23 (2011): pp. 1057–1066.
46. Sharkawi, A.M., and A.M. Seyam, *Mag. Concr. Res.* 71 (2019): pp. 637–646.
47. Yuan, Y., Y. Ji, and S.P. Shah, *ACI Struct. J.* 104 (2007): pp. 344–347.

10 FIGURE CAPTIONS

Figure 1 Surface resistivity of concrete made with various binders (without steel reinforcement)

Figure 2 Phases of iron oxides with their expansion (adapted from Hansson et al., 2012)

Figure 3 (a) Schematic and (b) photograph of the IC test setup

Figure 4 Effect of potential application (15 V) in the three sets T1, T2, and T3

Figure 5 Cracking in OPC, PFA, and LC3 specimens (Cracks are highlighted with marker for clarity)

Figure 6 Steel surfaces of IC test specimens showing form and degree of corrosion

Figure 7 Raman spectra of corrosion products of steel in OPC, PFA, and LC3 - after the Impressed Corrosion tests

Figure 8 Porosity at the S-B interface measured using MIP (after the corrosion tests)

Figure 9 Evidence of microstructural changes in concrete cover due to prolonged application of voltage in LC3 specimens

Figure 10 (a) Photograph of the test specimen, (b) and (c) Schematic diagram and photograph of natural diffusion (NC) test setup (Note: Nickel-Chromium mesh (CE) not shown in photograph for clarity of the image)

Figure 11 Typical linear polarization resistance (LPR) curve

Figure 12 Effect of binders on the corrosion current density

Figure 13 Pitting corrosion observed after the NC tests.

Figure 14 Raman spectra of corrosion products of steel in the OPC, PFA, and LC3 - after the Natural Corrosion tests

Figure 15 Instantaneous chloride and electrochemical conditions during corrosion tests

11 TABLES

Table 1 Resistivity (measured using Wenner 4 – probe surface resistivity test) of OPC, PFA and LC3 concretes used in the present study

Table 2 Formation of corrosion products in the presence of chlorides

Table 3 Chemical composition of steel used

Table 4 Oxide composition of the binders used

Table 5 Mixture proportions designed as per IS 456-2000 and properties of the concretes used

Table 6 Test groups and number of specimens tested

Table 7 Summary on the form of corrosion and corrosion products found after IC and NC tests

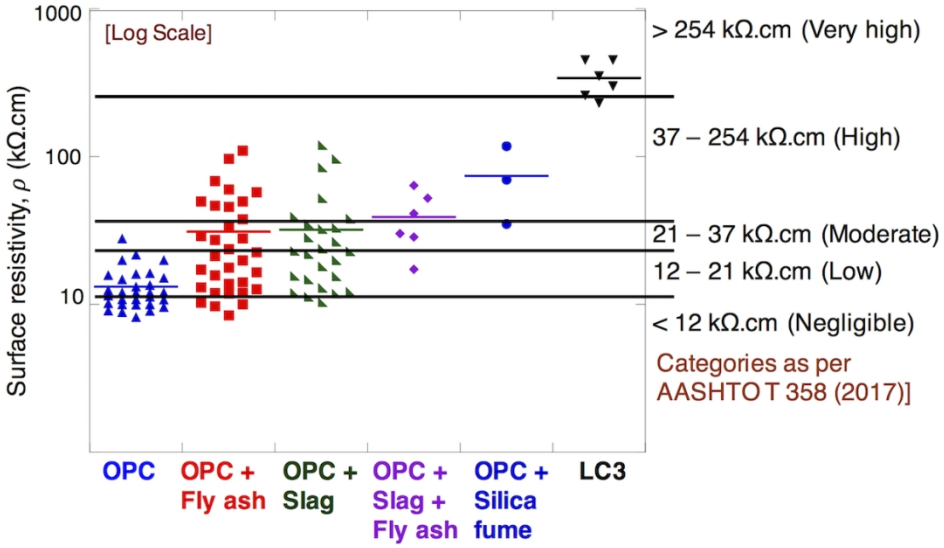

Figure 1 Surface resistivity of concrete made with various binders(without steel reinforcement)

83x48mm (400 x 400 DPI)

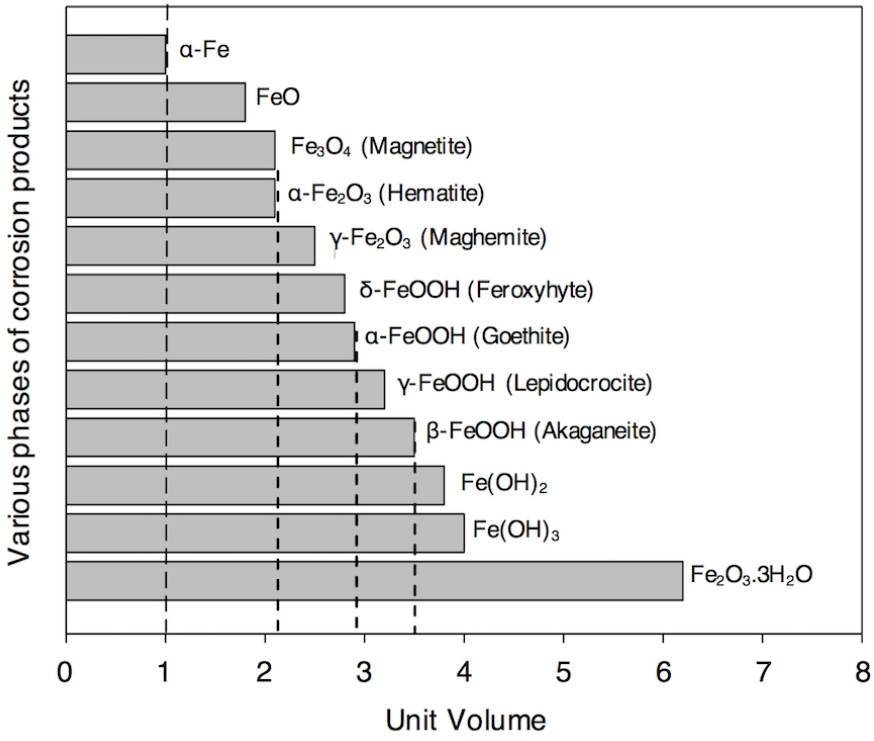

Figure 2 Phases of iron oxides with their expansion (adapted from Hansson et al., 2012)

83x66mm (300 x 300 DPI)

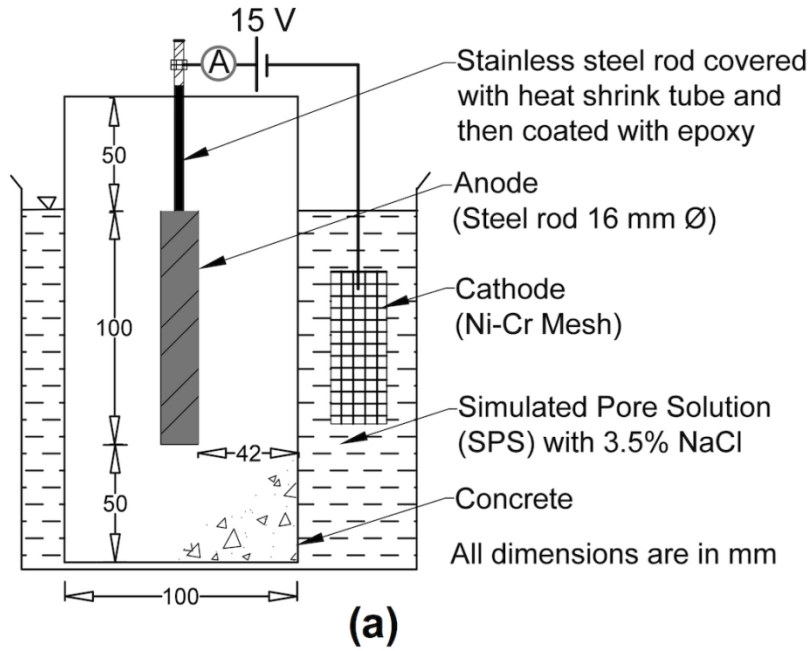

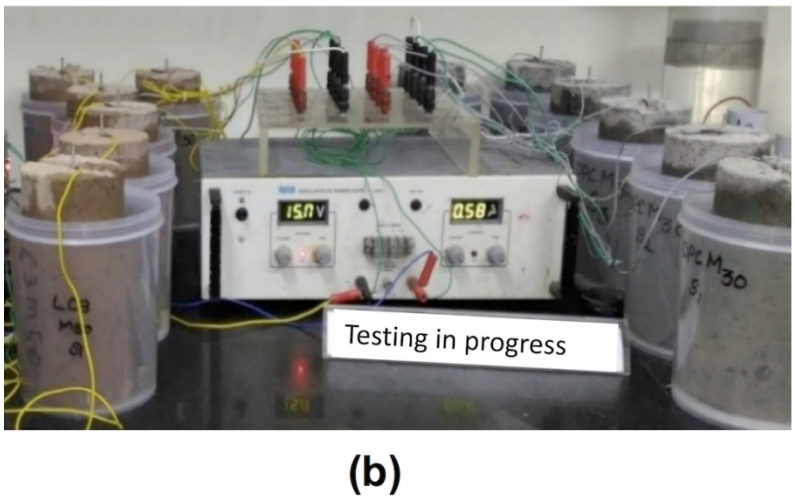

Figure 3 (a) Schematic and (b) photograph of the IC test setup

88x132mm (300 x 300 DPI)

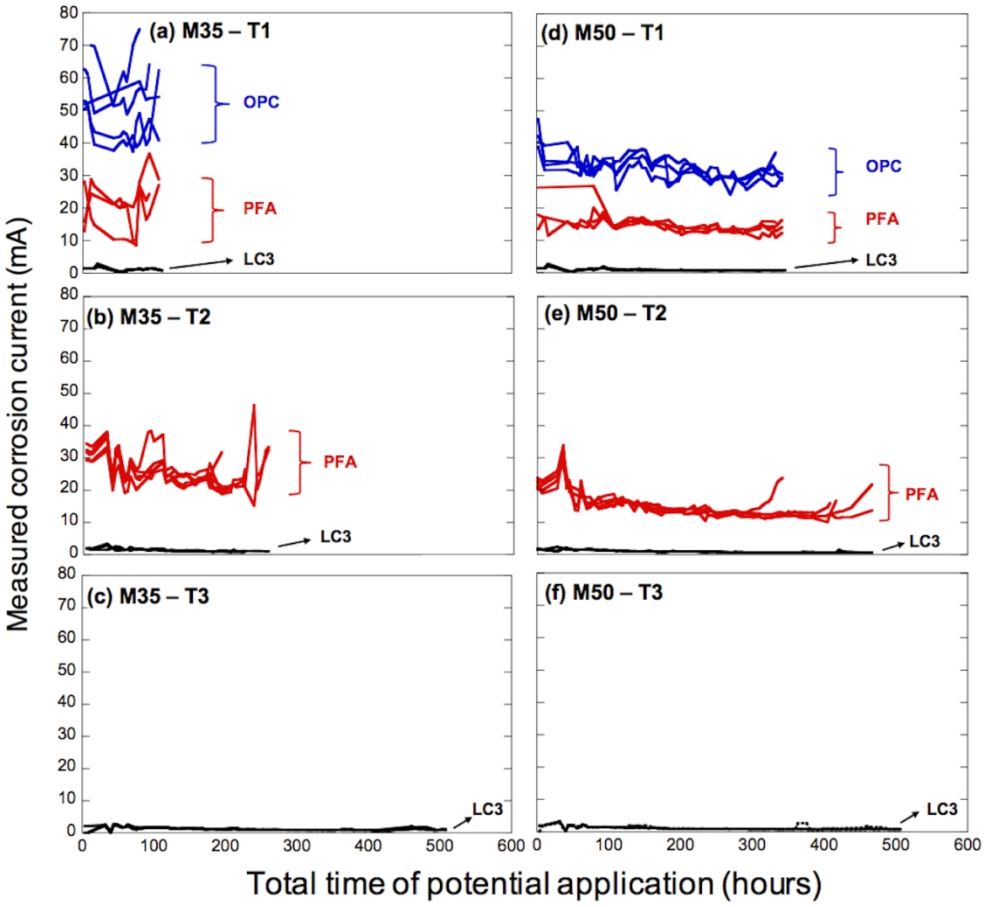

Figure 4 Effect of potential application (15 V) in the three sets T1, T2, and T3

169x152mm (200 x 200 DPI)

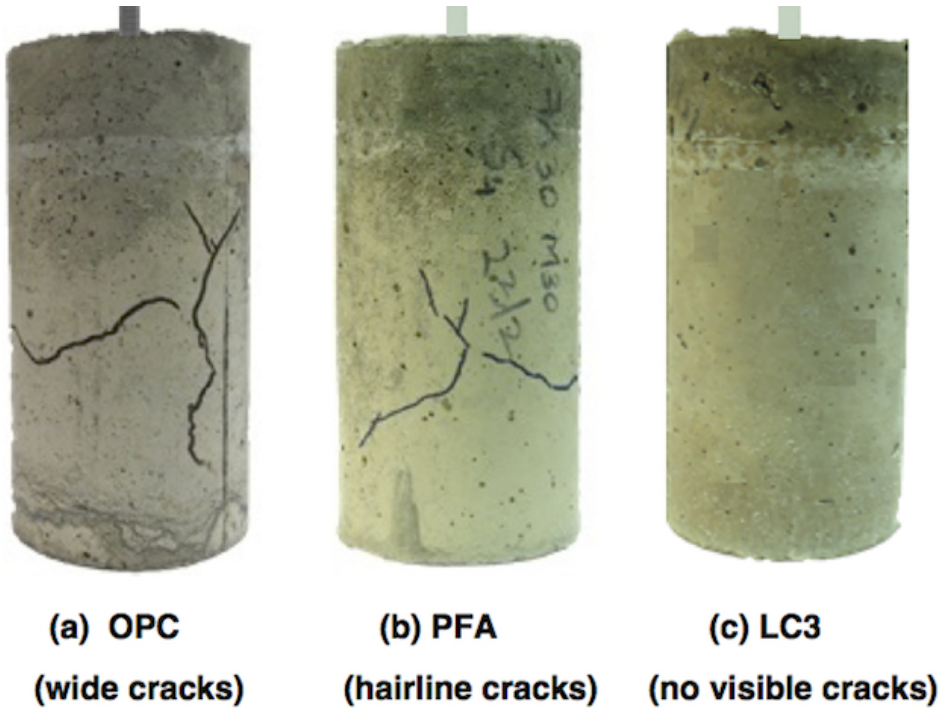

Figure 5 Cracking in OPC, PFA, and LC3 specimens

83x61mm (200 x 200 DPI)

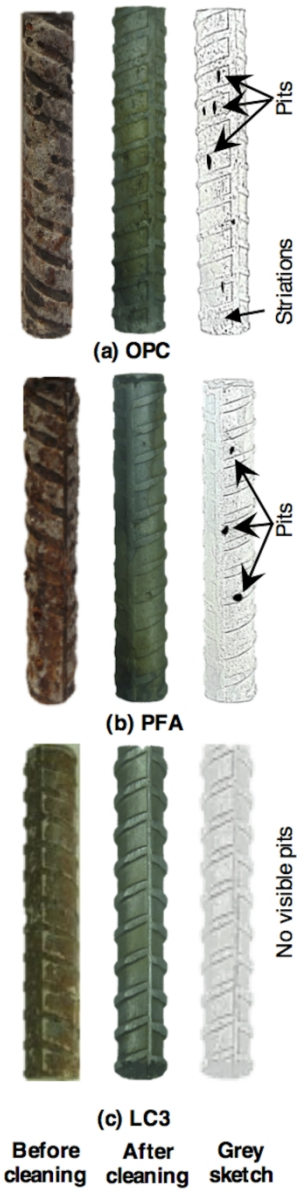

Figure 6 Steel surfaces of IC test specimens showing form and degree of corrosion

83x335mm (200 x 200 DPI)

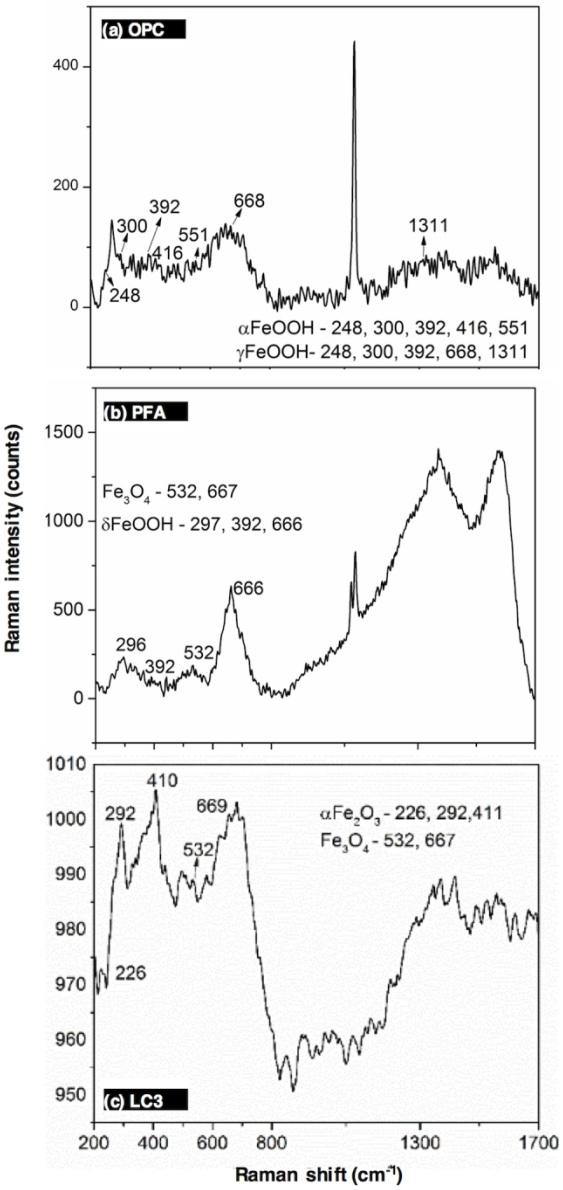

Figure 7 Raman spectra of corrosion products of steel in OPC, PFA, and LC3 - after the Impressed Corrosion tests

83x174mm (300 x 300 DPI)

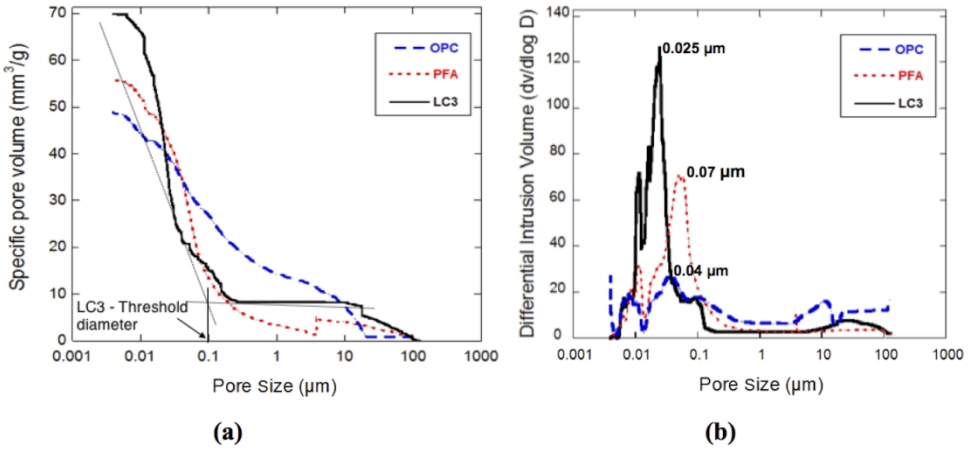

Figure 8 Porosity at the S-B interface measured using MIP (after the corrosion tests)

165x89mm (300 x 300 DPI)

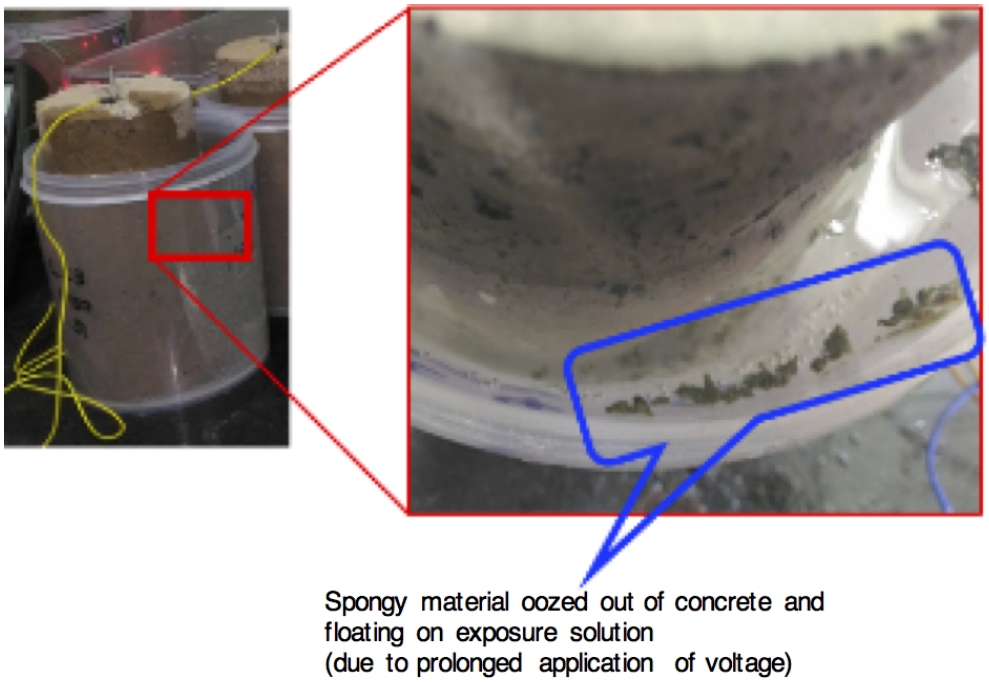

Figure 9 Evidence of microstructural changes in concrete cover due to prolonged application of voltage in LC3 Specimen

80x55mm (300 x 300 DPI)

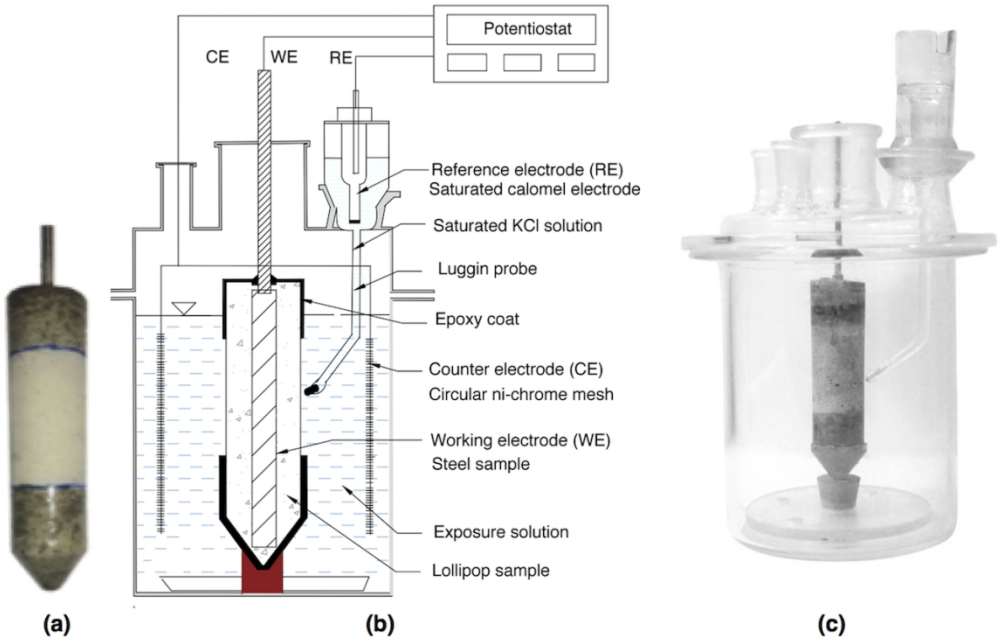

Figure 10 (a) Photograph of the test specimen, (b) and (c) Schematic diagramme and photograph of natural diffusion (NC) test setup (Note: Nickel-Chromium mesh (CE) not shown in photograph for clarity of the image)

169x122mm (200 x 200 DPI)

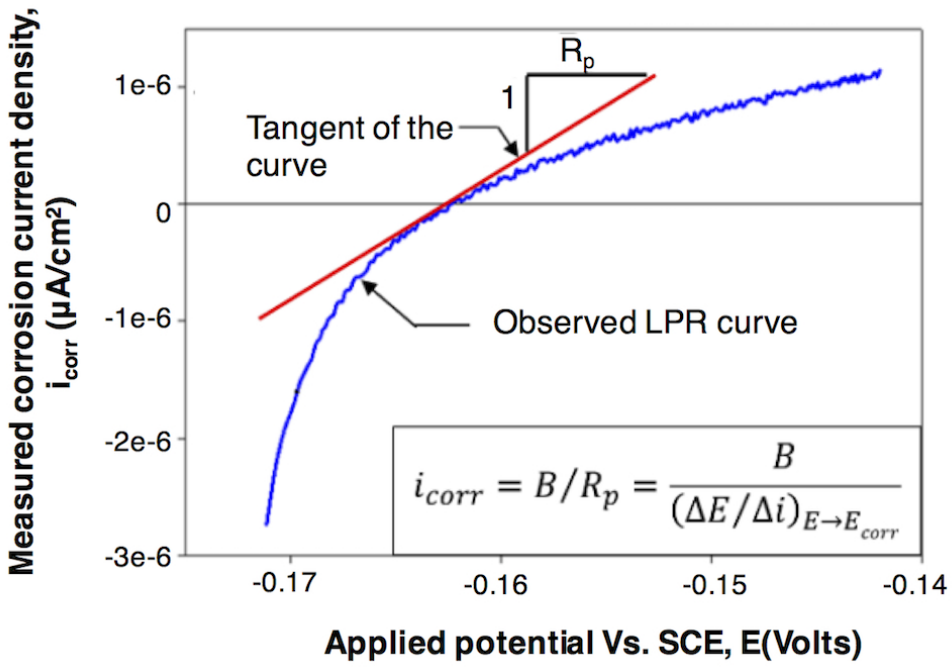

Figure 11 Typical linear polarization resistance (LPR) curve

83x60mm (300 x 300 DPI)

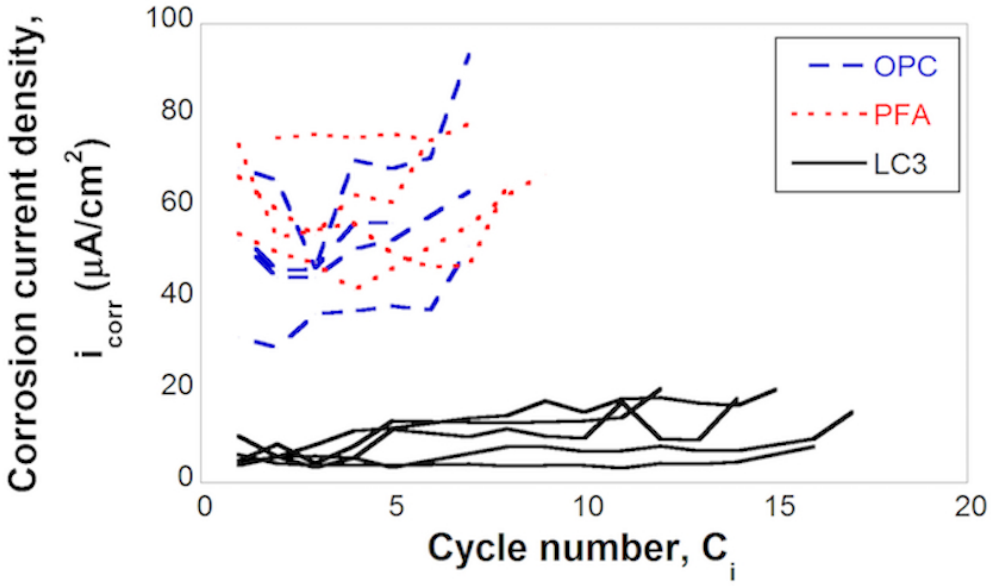

Figure 12 Effect of binders on the corrosion current density

71x43mm (300 x 300 DPI)

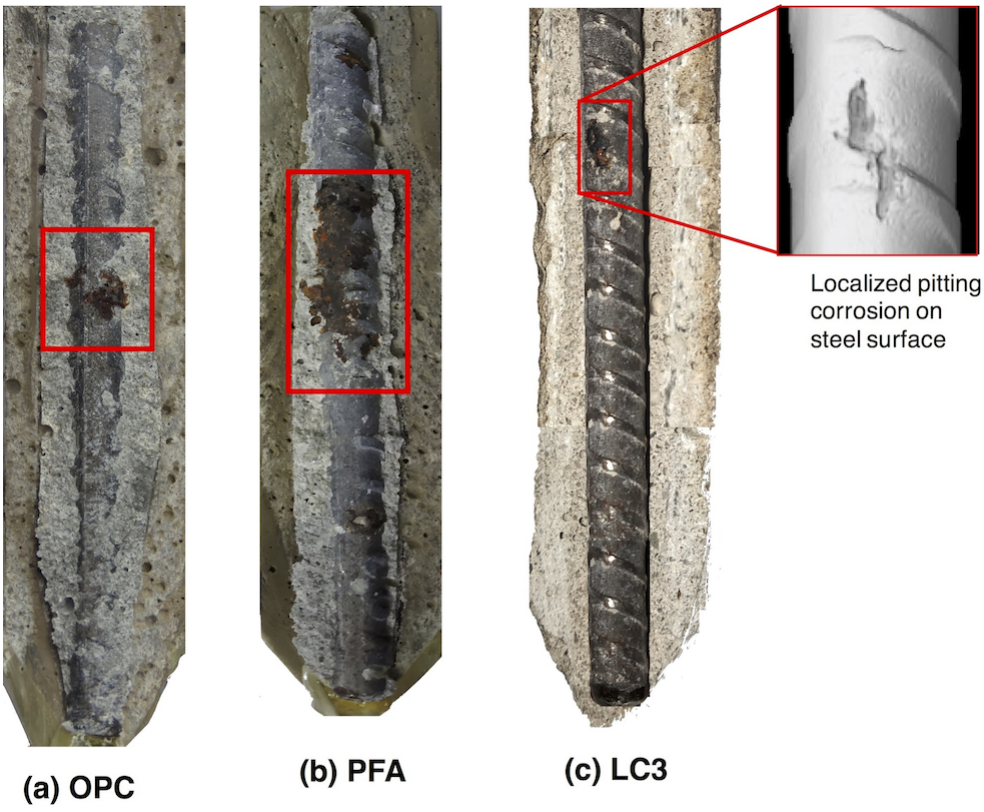

Figure 13 Pitting corrosion observed after the NC tests.

84x74mm (300 x 300 DPI)

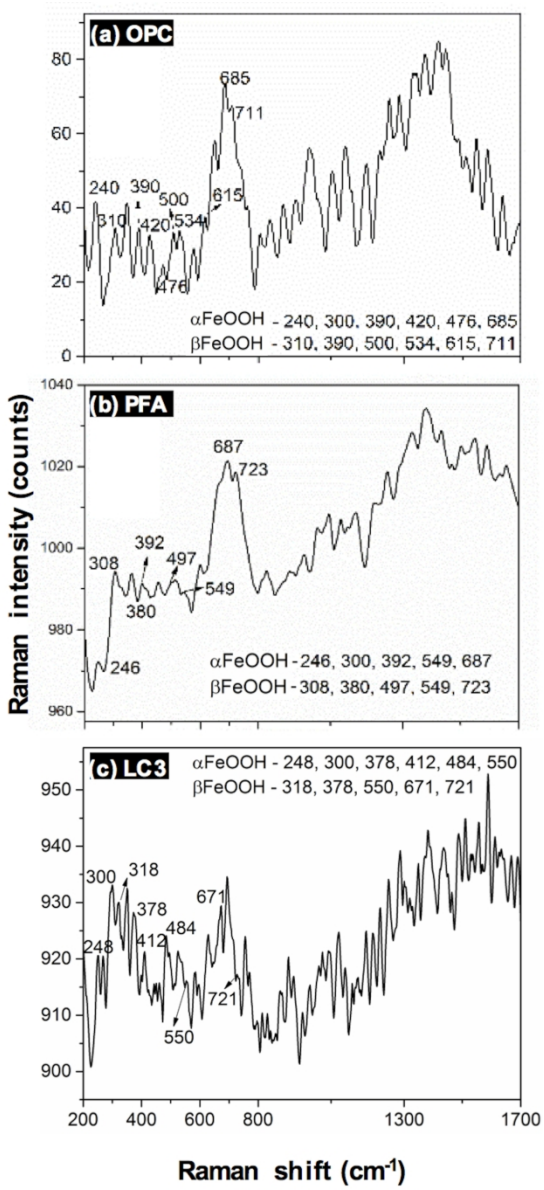

Figure 14 Raman spectra of corrosion products of steel in the OPC, PFA, and LC3 - after the Natural Corrosion tests

84x177mm (600 x 600 DPI)

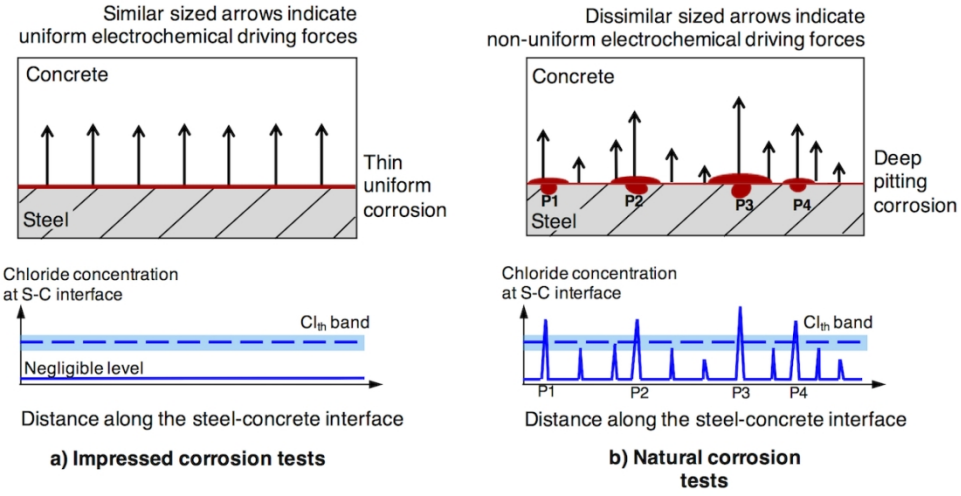

Figure 15 Instantaneous chloride and electrochemical conditions during corrosion tests

167x85mm (200 x 200 DPI)

Table 1 Resistivity (measured using Wenner 4 – probe surface resistivity test) of OPC, PFA and LC3 concretes used in the present study

Grade of concrete	Type of binder	Average surface resistivity (CoV) (kΩ.cm)		
		28 days	56 days	90 days
M35	OPC	11.1 (0.1)	11.9 (0.1)	11.5 (0.1)
	PFA	16.4 (0.1)	31.1 (0.1)	45.4 (0.1)
	LC3	227.5(0.1)	305.8 (0.1)	324 (0.1)
M50	OPC	15.3 (0.05)	16 (0.1)	18.6 (0.2)
	PFA	19 (0.1)	35.6 (0.1)	56.3 (0.1)
	LC3	298.6 (0.1)	316 (0.1)	428.6 (0.05)

* CoV – Coefficient of Variation

Table 2 Formation of corrosion products in the presence of chlorides

Initial product	Later products formed and the nature of products	Ref.
Passive layer	Magnetite (Fe_3O_4) / Hematite (α-Fe_2O_3) →During the initial phase of curing, an inner layer composed of magnetite and outer layer with oxygen availability composed of hematite is formed. Presence of hematite gives the orange color to the rust. Formation of hematite or magnetite does not induce significant cracking as these oxides occupy only twice volume of steel and displace readily	Marcotte et al., 2007
Green rust I	Hematite → Green rust can dissolve in pore solution and ooze out through the pore spaces in concrete and on exposure to atmosphere forms hematite.	
	Feroxyhyte (δ-FeOOH) → If the concentration of chloride is low, then Feroxyhyte is formed. 3 times increase in volume is observed.	Sagoe-Cretsil and Glasser, 1993
	Akagenite (β-FeOOH) → If the concentration of chloride is very high, then Akagenite is formed. 3.5 times increase in volume is observed.	
	Lepidocrocite (γ-FeOOH) → If the electrochemical potential is high, then Lepidocrocite is formed. 3.1 times increase in volume is observed.	
Lepidocrocite	Amorphous ferric oxyhydroxide → Lepidocrocite converts to an intermediate unstable product when the surrounding pH reduces	Criado et al., 2015
Amorphous ferric oxyhydroxide	Goethite (α-FeOOH) → 2.9 times increase in volume	

Table 3 Chemical composition of steel used

Element	Composition (%)
C	0.25
Si	0.378
Mn	0.66
P	0.02
S	0.017
Cr	0.058
Ni	0.032
Cu	0.016
Al	< 0.008
B	< 0.001
Nb	0.05
Pb	< 0.02
Ti	0.005
W	< 0.005
N	0.007
Fe	98.492
Total*	99.985

*Excluding other trace elements

Table 4 Oxide composition of the binders used

Oxides	Concentration (%)				
	OPC	Class F fly ash	Limestone Calcined Clay Cement (LC3)		
			Clinker	Calcined Clay	Limestone
Al_2O_3	4.17	29.95	5.24	24.95	1.74
CaO	64.59	1.28	63.81	0.09	48.54
Fe_2O_3	3.89	4.32	3.41	5.08	1.62
K_2O	0.59	1.44	0.19	0.21	0.13
MgO	0.88	0.61	3.06	0.19	0.467
Na_2O	0.16	0.16	0.32	0.05	-
SiO_2	19.01	59.32	21.12	58.43	10.07
SO_3	1.7	0.16	0.63	-	0.01
TiO_2	0.23	0.206	-	0.10	1.41
LOI	1.4		0.98	9.58	37.09

Table 5 Mixture proportions as per IS 456-2000 and properties of the concretes used

Materials		M35			M50		
Binder type		OPC	PFA	LC3	OPC	PFA	LC3
Binder content (kg/m^3)		310	310	310	360	380	440
Fine aggregate (kg/m^3)		764	777	770	718	714	695
Coarse aggregate (kg/m^3) (maximum size = 20 mm)		1171	1221	1253	1172	1167	1213
Water-binder ratio		0.50	0.45	0.45	0.40	0.35	0.35
28-day cube compressive strength	Mean (MPa)	45.7	45	44.6	62.8	53.0	54.0
	CoV	0.08	0.1	0.03	0.03	0.04	0.03
28-day splitting tensile strength	Mean (MPa)	7.2	6.7	6.9	7.8	8.2	7.7
	CoV	0.05	0.06	0.03	0.05	0.1	0.09

* CoV – Coefficient of Variation

Table 6 Test groups and number of specimens tested

Test group	M35			M50		
	OPC	PFA	LC3	OPC	PFA	LC3
T1	5	5	5	5	5	5
T2		5	5		5	5
T3			5			5

Table 7 Summary on the form of corrosion and corrosion products found after IC and NC tests

	Impressed corrosion (IC) tests			Natural corrosion (NC) tests		
	OPC	PFA	LC3	OPC	PFA	LC3
Corrosion products	α-FeOOH; γ-FeOOH	δ-FeOOH; Fe_3O_4	α-Fe_2O_3; Fe_3O_4	β-FeOOH		
Form of corrosion	Uniform corrosion			Pitting corrosion		